

Novel fusion method for SAR and optical images based on non-subsampled shearlet transform

Tianyong Chu, Yumin Tan, Qiang Liu & Bingxin Bai

To cite this article: Tianyong Chu, Yumin Tan, Qiang Liu & Bingxin Bai (2020) Novel fusion method for SAR and optical images based on non-subsampled shearlet transform, International Journal of Remote Sensing, 41:12, 4590-4604, DOI: [10.1080/01431161.2020.1723175](https://doi.org/10.1080/01431161.2020.1723175)

To link to this article: <https://doi.org/10.1080/01431161.2020.1723175>



Published online: 20 Feb 2020.



Submit your article to this journal [↗](#)



Article views: 33



View related articles [↗](#)



View Crossmark data [↗](#)



Novel fusion method for SAR and optical images based on non-subsampled shearlet transform

Tianyong Chu, Yumin Tan, Qiang Liu and Bingxin Bai

Department of Civil Engineering, Beihang University, Beijing, China

ABSTRACT

Due to the different imaging modes of SAR images and optical images, traditional image fusion methods are no longer suitable for the fusion of the two types of images. Fused images often have problems of spectral distortion and excessive introduction of noise. This study proposes an improved SAR-optical images fusion algorithm based on non-subsampled shearlet transform (NSST). NSST decomposition is first performed on the two types of images. Then, in the low-frequency sub-band of the decomposition image, a weighted average fusion rule using the coefficient of variation according to the different imaging characteristics of SAR images and optical images is proposed to avoid spectral distortion. In the high-frequency sub-band of the decomposition image, the effect of SAR image noise on the fused image is removed by setting the coherence coefficient threshold. The subjective visual assessment and objective index evaluation on the experimental results both show that the fusion results using the proposed algorithm are significantly improved. The proposed algorithm smoothly fuses the detailed information of the SAR image into the optical image without the excessive introduction of noise while maintaining the spectral information of the optical image. Meanwhile, the proposed algorithm has a relatively simpler mathematical structure compared to the algorithm based on sparse representation, thus reducing the operating time and manual work.

ARTICLE HISTORY

Received 22 May 2019

Accepted 12 December 2019

1. Introduction

Image fusion is an important research topic in the image processing field which has a great research potential and promising future. Image fusion technology extracts important information from images acquired by multiple sensors or in variety of ways, and then combines them through specific processing methods and fusion rules to obtain fused images (Kong, Zhang, and Lei 2014). The results can provide rich and efficient information that cannot be obtained from a single sensor. It has been widely applied to various fields, such as multi-focus image fusion (Li et al. 2018; Haghghat, Aghagolzadeh, and Seyedarabi 2011), remote sensing image fusion (Li et al. 2017; Zhang and Zhang 2018; Ghahremani and Ghassemian 2015; Wang et al. 2017), and medical image fusion (Zhang et al. 2016; Bhatnagar, Wu, and Liu 2013).

CONTACT Tianyong Chu ✉ 13131229@buaa.edu.cn Department of Civil Engineering, Beihang University, Beijing, China

In the field of remote sensing image fusion, the fusion of synthetic aperture radar (SAR) and optical images is a hot and difficult issue. SAR and optical images have different imaging modes and their respective advantages and disadvantages. SAR is a kind of active remote sensing sensor. It acquires images by emitting electromagnetic waves to the ground and receiving reflected echoes from the target. SAR images contain rich and detailed texture information. The advantage of SAR is that it has strong penetrating power and thus not affected by cloud or rain. Moreover, it can acquire images at night without relying on the sunlight. But it also has drawbacks. Electromagnetic waves emitted by SAR have only one single band. Therefore, it is impossible to visually interpret the surface condition due to less spectral information on a single-band greyscale image (Brekke and Solberg 2005). Optical sensor is a passive remote sensing equipment. It obtains images by receiving reflections of sunlight from the ground objects. Optical images have abundant spectral information but less detailed texture information. In summary, the images captured by SAR and optical sensors provide complementary information and need to be fused for better interpretation and analysis. The research of SAR and optical image fusion is of great importance and has been applied in many fields, such as land use mapping (Ban, Hu, and Rangel 2010; Wang and Glennie 2015), target extraction (Kim, Song, and Kim 2018; Errico et al. 2015) and change detection (Ban, Hu, and Rangel 2007; Borghys, Shimoni, and Perneel 2007).

However, the different imaging modes of SAR and optical sensors bring challenges to data fusion (Joshi et al. 2016). Therefore, traditional image fusion methods like Brovey, IHS, PCA, and SVR are no longer suitable for the fusion of these two kinds of images (Yi, Zeng, and Yuan 2018). Researchers mostly use the multi-scale transformation method for SAR-optical image fusion. Multi-scale transformation mainly includes wavelet transform non-subsampled contourlet transform theory (NSCT) and non-subsampled shearlet transform (NSST). In 2000, Tang (Tang, Wang, and Huang 2000) implemented wavelet transform to SAR-optical images for data fusion. However, the multi-scale decomposition of the wavelet transform is only in a few directions, making it difficult for the fusion results to reflect good spatial edge information. In Do and Vetterli 2005, Do and Vetterli proposed the Contourlet transform and used it for SAR-optical image fusion. Although the transformation overcomes the limitation of finite directions, its multi-scale decomposition does not have translation invariance, and the fused image is prone to Gibbs phenomenon. After that, Cunha (Da Cunha, Zhou, and Do 2006) proposed NSCT, which was mainly achieved by improving the Contourlet transform. Easley (Easley, Labate, and Lim 2008) developed the NSST transformation method. Compared with NSCT, NSST can avoid the Gibbs phenomenon while effectively maintaining the spatial texture and the details of the image. In addition, NSST has a simpler mathematical structure which makes it more efficient. Currently, NSST is one of the most advanced multi-scale transformation methods. In 2018, Sheng (Sheng, Yang, and Dong 2018) applied NSST to SAR and optical image fusion. The author used sparse representation to develop fusion rules and achieved good results. However, the SAR images the author used are simple and have less noise. Furthermore, the algorithm based on sparse representation is relatively complex and inefficient.

In order to make better use of the increasingly popular SAR images and reduce code-running time, we develop a novel fusion algorithm for SAR-optical images. We first perform NSST decomposition on the SAR images and the luminance components of the

optical images to get low-frequency sub-band and high-frequency sub-band. Then, for low-frequency coefficients, we design a weighted average fusion rule considering the coefficient of variation (CV) according to the different imaging models of the SAR-optical images. For high-frequency coefficients, we set a coherence coefficient threshold to remove the effect of SAR image noise on the fused image. As a result, on the one hand, the fused image maintains the spectral characteristics of the optical image well. On the other hand, the detailed texture information of the SAR image is smoothly fused into the fused image without the effect of SAR noise. At the same time, the proposed algorithm is relatively simple and more efficient.

2. Methods

2.1. HSI transformation

The SAR image is a greyscale image with brightness information. The optical image is a colour image expressed in the RGB space. For the fusion of optical images, we often want to retain its rich spectral information. Colour models are used to segment and extract the components of spectral information. However, in the RGB colour model, the three basic colours are unevenly distributed in space, and they represent not only colour information but also brightness information, which can easily cause loss or confusion of other component information when processing one of the components. Thereby, the SAR-optical images cannot be directly fused in the RGB space. Otherwise, it will cause serious spectral distortion.

HSI (hue, saturation, and intensity) is a colour space created in the way human visual systems perceive colour. The H (hue) and S (saturation) components represent the chrominance information of the image, while the I (intensity) component represents the brightness information of the image. The HSI colour model is chosen to describe the image because it can separate the chrominance and luminance information of the image. The I component of the optical image is used to be fused with the SAR image separately. It can maintain the spectral information of the optical image and prevent the occurrence of spectral distortion.

2.2. Non-subsampled shearlet transform

The NSST transform is a non-orthogonal transform. Its discretization process is described as follows: Firstly, the not sampling Pyramid (NSP) scale decomposition is performed to obtain the low-frequency sub-band image and the high-frequency sub-band image. Then, the high-frequency sub-band image of each stage is processed with the shear filter (SF) to obtain the sub-band image information in different directions (Singh et al. 2015).

For a continuous wavelet, a two-dimensional affine system with composite dilations is defined in Formula (1) (Easley, Labate, and Lim 2008):

$$M_{AS}(\Psi) = \left\{ \Psi_{j,k;i}(x) = |\det A|^{j-2} \psi(S^k A^j x - i) : j; k \in \mathbb{Z}; i \in \mathbb{Z}^2 \right\} \quad (1)$$

where A represents the dilation matrix, S is the shear matrix, j , k , and i denote scale, direction, and shift parameter, respectively $\Psi \in L^2(\mathbb{R}^2)$. A and S are 2×2 invertible

matrices and $|\det S| = 1$. $A = \begin{pmatrix} a & 0 \\ 0 & \sqrt{a} \end{pmatrix}$ and $S = \begin{pmatrix} 1 & s \\ 0 & 1 \end{pmatrix}$, where 'a' is the shearlet scale and 's' controls the shearlet direction.

Firstly, Multi-scale decomposition is performed i times to form $(i+1)$ sub-band images, which include one low-frequency component and i high-frequency components. All the sub-band images are of the same size as the source image. Then, multi-directional decomposition is applied to all the high-frequency sub-band images obtained by each level multi-scale decomposition. The SF used for directional decomposition is obtained by directly mapping a standard SF from pseudo-polarized grid system to Cartesian coordinates system. After Fourier transform, the two-dimensional convolution operation is realized. In this way, the subsampled step of the standard SF is avoided and the new SF is translation invariant. In this study, the source images are processed with four-level NSST decomposition. The numbers of shear directions are 4, 4, 8, and 8 from the low level to the high level. For example, the process of two-level multi-scale and multi-directional decomposition of NSST is illustrated as in Figure 1, which is modified from (Singh et al. 2015).

2.3. Fusion rules

2.3.1. Low-frequency coefficient

The low-frequency coefficients of the image preserve the primary energy and express the body contour of the source image (Huang, Bi, and Wu 2018). Low-frequency images are blurry and rarely contain noise. Figure 2 shows that the low-frequency sub-band images of SAR and optical images are quite different. They have opposite polarity on some ground objects. For example, rivers have low pixel values on SAR images but high pixel values on optical images. This is because SAR actively emits electromagnetic waves to the ground at a certain oblique angle. The incident wave mainly produces mirror reflection on the surface of the river with little backscattering. Therefore, the design of the low-frequency coefficient fusion rule plays a decisive role in the spectral preservation of optical images. In Sheng, Yang, and Dong 2018, a sparse representation fusion rule based on structure similarity and luminance difference was used in low-frequency fusion.

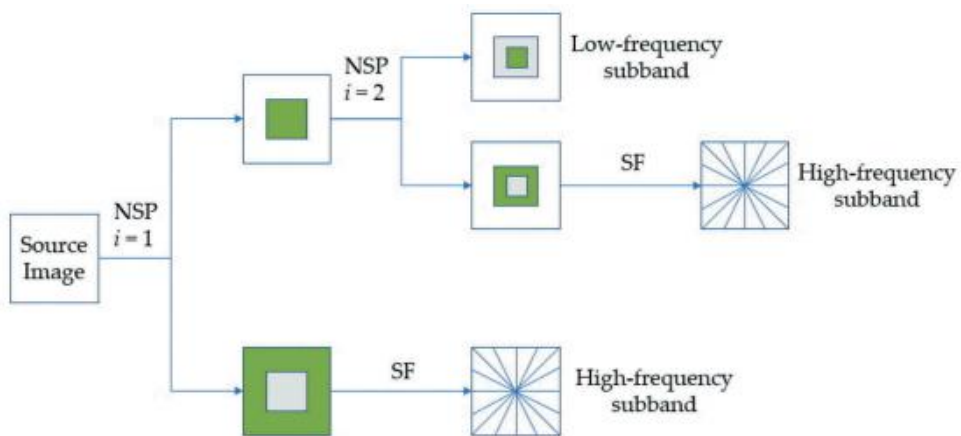


Figure 1. Two-level multi-scale and multi-directional decomposition of the NSST.

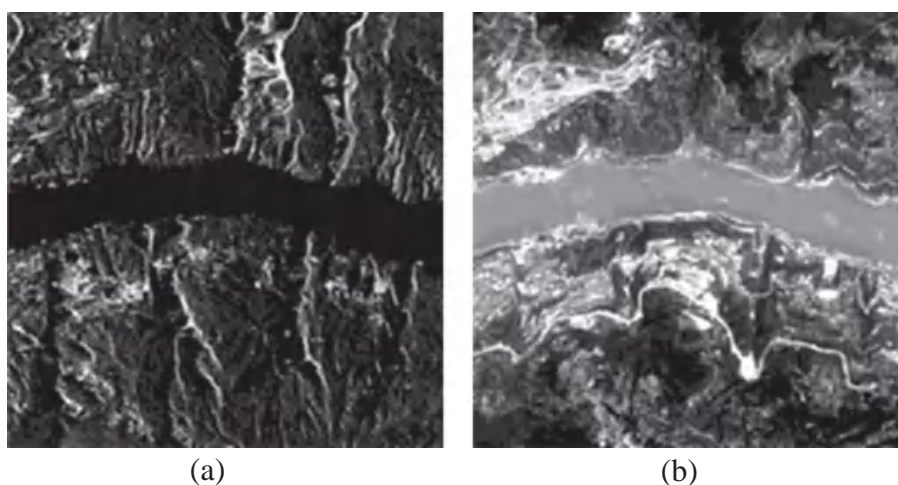


Figure 2. Low-frequency sub-band images (a) The source image is the SAR image (Palsar-2); (b) The source image is an optical image (Sentinel-2A).

The fusion results were good with little spectral distortion. But the sparse representation fusion rule is very complex. It needs to build a training set with additional SAR and optical images to obtain an over-complete dictionary. Furthermore, the sparse representation of low-frequency coefficients using the dictionary requires a great amount of calculations. In this research, a relatively simpler fusion rule, adaptive weighted averaging, is proposed in low-frequency fusion, which saves both labour and time. In the proposed low-frequency fusion rule, the determination of weight is the key to maintain spectral characteristics. We use coefficient of variation (C_v) to determine the weight. Formula (2) gives the calculation of C_v (Stępnik 2011):

$$C_v = \frac{\sqrt{\frac{1}{n} \sum_{i=1}^n (x_i - \mu)^2}}{\mu} \quad (2)$$

where μ is the mean of all values. C_v expresses the degree of dispersion of a set of data. Used in images, it evaluates whether the image is smooth or not. Compared to standard deviation, C_v can compare data sets with large differences. As aforementioned, the same object may have opposite polarity in SAR and optical images. Direct fusion would cause spectral distortion. It can be determined whether the objects in the two low-frequency images are similar or not by comparing the 3×3 neighbourhood window C_v of two images, even they have opposite polarities in the two images. If the C_v of the SAR image is larger than that of the optical image, which means that the SAR image provides more useful information, the larger weight should be given to the SAR image to introduce more texture information. Otherwise, the larger weight should be given to the optical image to maintain spectral information. Formula (2) indicates that small disturbance may have a huge impact on C_v when the average value (μ), the denominator of the formula, is close to zero. But during image processing, the pixels whose mean of 3×3 neighbourhood window is close to zero won't provide more useful information. Therefore, the low-frequency coefficients of the optical image are used to be the fused coefficients at

these pixels. The specific process of the algorithm is as follows: Firstly, we calculate the C_v in the 3×3 neighbourhood of each pixel in the two low-frequency images to obtain the C_v matrices of the two images. Each value in the C_v matrix is calculated as in Formula (3):

$$C_{v;j;k} = \frac{\sqrt{\frac{1}{3 \times 3} \sum_{j=j-1}^{j+1} \sum_{k=k-1}^{k+1} (x_{j;k} - \bar{x})^2}}{\bar{x}} \quad (3)$$

Secondly, we subtract the optical C_v matrix from the SAR C_v matrix and the result is matrix C_{vd} . The values less than zero in the C_{vd} matrix is set to zero. Finally, a 2% linear stretch normalization is performed on the C_{vd} matrix. The resultant matrix is the weight matrix of SAR low-frequency coefficients.

2.3.2. High-frequency coefficient

The high-frequency coefficients of the images contain the detailed texture information (Cheng, Jin, and Li 2018). In Sheng, Yang, and Dong 2018, Sum of Modified Laplacian fusion rule was used in high-frequency fusion. Noise of SAR images was not considered in Sheng, Yang, and Dong 2018 because the SAR images used had little noise. However, it is very common for SAR images to exhibit noise as echoes from targets interfere with each other and may cause the appearance of salt-and-pepper known as speckle (Goodman 1976). Residential areas, in particular, display more noise because angular reflections would occur at buildings. Figure 3 shows the noise in residential areas of an SAR image. If the energy rule in Sheng, Yang, and Dong 2018 is used directly in residential areas, it will lead to the excessive introduction of SAR image noise. However, these areas have high coherence coefficient when doing the D-InSAR process. Therefore, in this research, we innovatively introduce a coherence coefficient threshold to reduce the introduction of SAR noise. If the coherence coefficient of a certain pixel is above the threshold, the high-frequency coefficient of the optical image will be used as the fused coefficient. Otherwise, the coefficient whose region energy in 3×3 neighbourhood is larger will be selected to be the fused coefficient.

3. Experiments

3.1. Study area and data

The study area is the Badong section of the Three Gorges Reservoir in the Yangtze River in Badong county, Hubei province, China. Its geographical coordinate range is from $31^{\circ}1'39''N$ to $31^{\circ}4'26''N$ and from $110^{\circ}19'55''E$ to $110^{\circ}23'11''E$. The image size is 6×6 km (2000×2000 pixels). The study area has complicated geological conditions with mountains, rivers, and residential areas. Experiments in this complicated region can prove the universality of our proposed algorithm.

In our experiments, the SAR image is PaISAR-2 in L-band with 3 m ground resolution. The optical image is Sentinel-2A with 10 m resolution. Two pairs of images acquired at different times are used in our experiments to avoid contingency. The first pair contains a PaISAR-2 SAR image and a Sentinel-2A optical image obtained on 15 August 2016 and 14 August 2016, respectively. The second pair contains a PaISAR-2 SAR image and a Sentinel-2A optical image captured on 5 June 2017 and 20 June 2017, respectively. The SAR images are pre-processed using filtering and geocoding. The optical images are

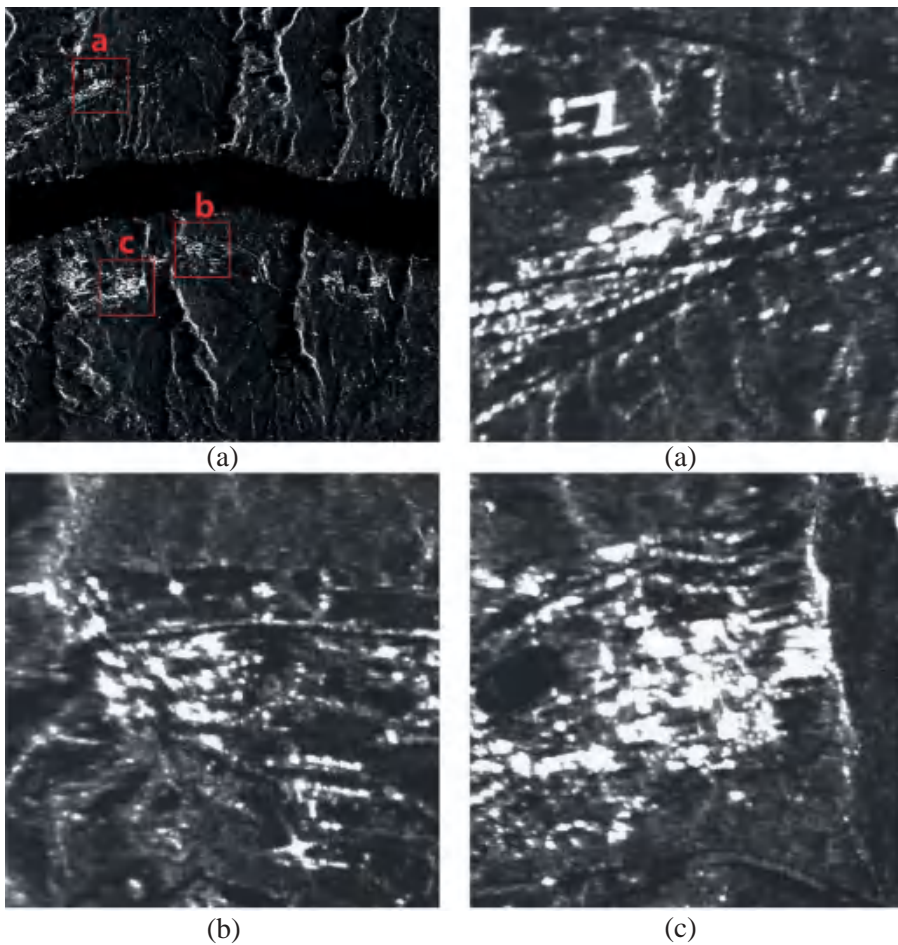


Figure 3. The noise in residential areas of an SAR image. (a), (b), and (c) are enlarged images of corresponding areas in (A).

pre-processed with radiometric calibration and atmospheric correction. All the images have been registered. [Figure 4](#) shows the images after pre-processing. The above processing procedures are completed in ENVI software package.

3.2. Experiment procedure

We fuse each pair of images, respectively (Experiment 1 and Experiment 2). For each pair, the procedure of the fusion experiment is illustrated in [Figure 5](#).

First, we perform HSI transformation on the optical image to obtain the I component of it. Second, the histogram of the SAR image is matched to that of the I component. Third, NSST decomposition is implemented to the SAR and I images to get the high- and low-frequency coefficients, respectively.

Before the high-frequency fusion, we obtain the coherence coefficients by doing D-InSAR process on the SAR image. As mentioned above, a coherence coefficient

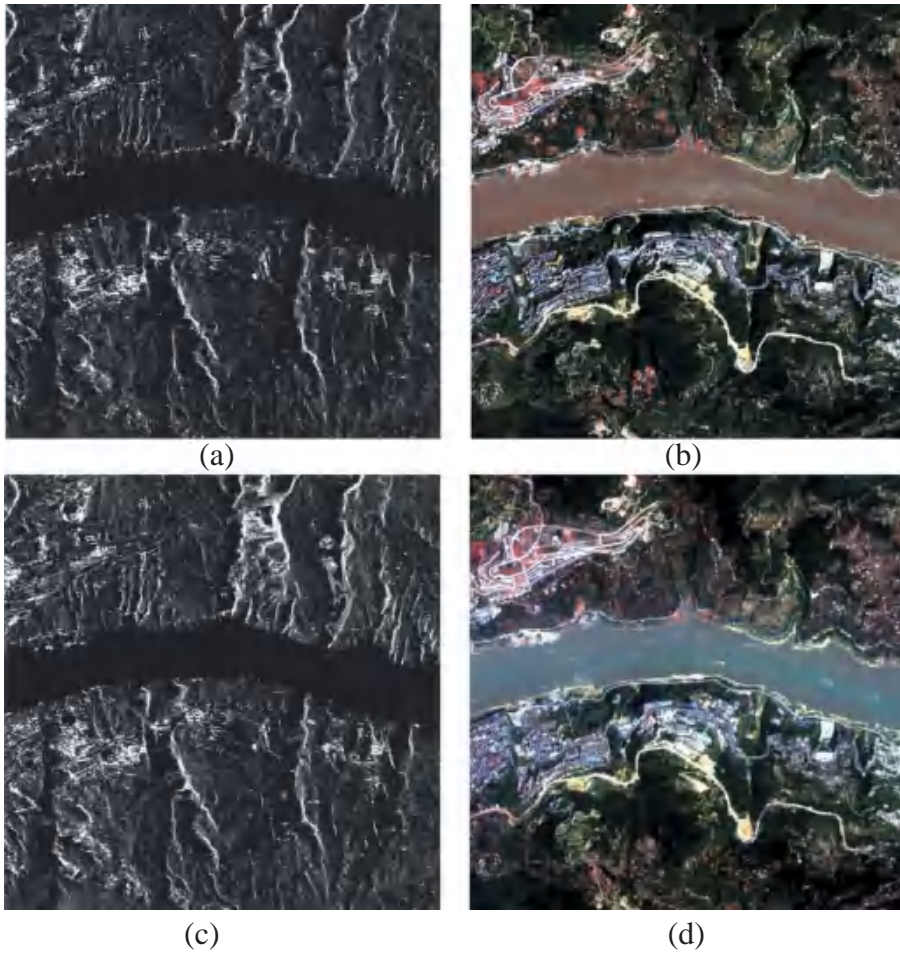


Figure 4. Images used in fusion experiments. (a) PalSAR-2 SAR image acquired on 15 August 2016; (b) Sentinel-2A optical image acquired on 14 August 2016; (c) PalSAR-2 SAR image acquired on 5 June 2017; and (d) Sentinel-2A optical image acquired on 20 June 2017.

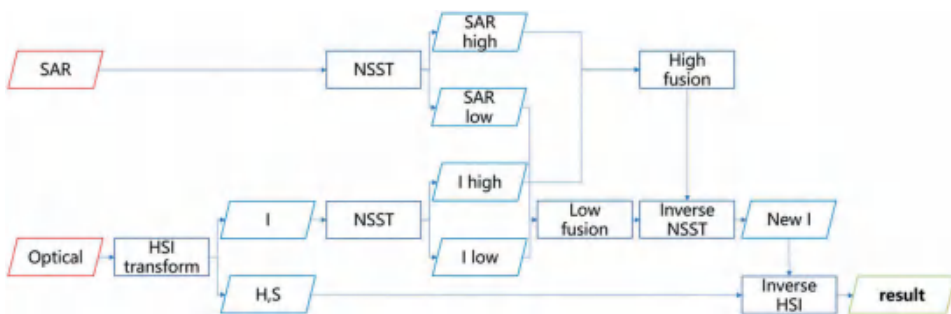


Figure 5. Flow chart of fusion experiment.

threshold needs to be determined to limit the excessive introduction of SAR image noise. We randomly select 5,000 pixels in the residential area, river, and forest, respectively, and count the coherence of each class to obtain their coherence histograms (Figure 6). The mode of the coherence coefficient of the residential area is selected to be the threshold, which is about 0.8. This value is almost greater than all the coherence values of the river and forest. It means that this threshold wouldn't limit the introduction of other useful information in the river and forest.

Then, high-frequency coefficients of the SAR and I images are fused using the high-frequency fusion rules, while low-frequency coefficients are fused using the proposed low-frequency fusion rules. After that, all the fused sub-band coefficients are processed with inverse NSST to get the new I component. Finally, the new I component is processed with inverse HSI transformation together with the H and S components obtained before, resulting in the final fused image.

4. Results and discussion

4.1. Subjective evaluation

The original images of Experiment 1 are the PaISAR-2 image and the Sentinel-2A image acquired on 15 August 2016 and 14 August 2016, respectively. The resultant images fused with NSCT, NSST, the algorithm in Sheng, Yang, and Dong 2018 and our proposed algorithm are shown in Figure 7. The original images of Experiment 2 are the PaISAR-2 image and the Sentinel-2A image captured on 5 June 2017 and 20 June 2017,

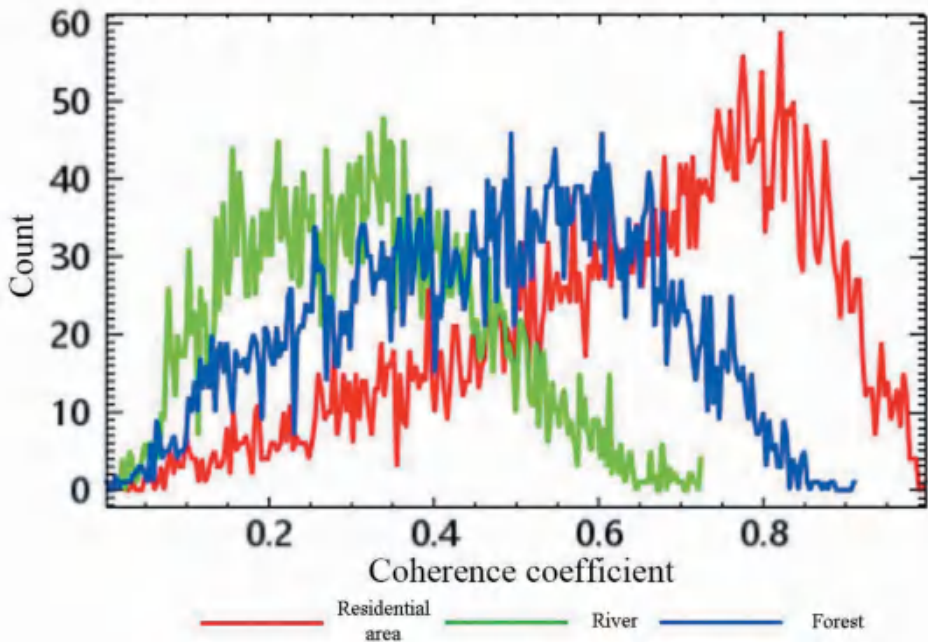


Figure 6. Coherence coefficient histograms of the residential area, river, and forest.

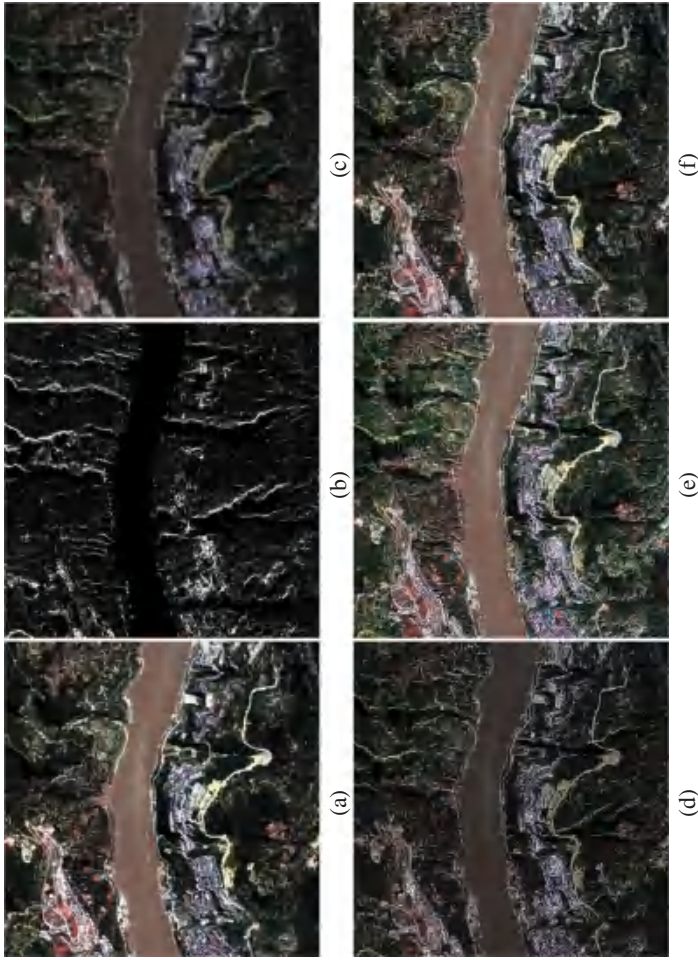


Figure 7. Fusion results of Experiment 1. (a) The original optical image; (b) The original SAR image; (c) Fusion result with NSCT; (d) Fusion result with NSST; (e) Fusion result with the algorithm in Sheng, Yang, and Dong 2018; and (f) Fusion result with our proposed algorithm.

respectively. And the resultant images using the above four different algorithms are shown in Figure 8.

Figure 7 and Figure 8 show that the NSCT algorithm results are blurred and the details are not prominent. The images are dark overall and certain spectral distortion can be discerned. There is also some excessive introduction of noise in residential areas.

The NSST results are sharper than the NSCT results and contain more detailed information. But they still exhibit spectral distortion. Especially in Experiment 2, severe spectral distortion occurs in some places which are dark in the original image such as the area in red rectangle in Figure 8. This is because that the I component pixel values in dark areas are close to zero, which means there is almost no spectral information here. If SAR information is introduced, the spectral distortion would inevitably occur. The NSST results also display more severe SAR noise than the NSCT results in residential areas. Because NSST has excellent high-frequency detail-capturing capability, SAR noise in residential areas is introduced in large quantities in the high-frequency part.

The algorithm in Sheng, Yang, and Dong 2018 produces quite good visual effect in the results. However, much noise appears in residential areas due to the no consideration of speckle in the SAR image.

The results fused with our proposed algorithm show accurate spectral information similar to that of the original optical image. It is because that CV is used to determine the weight of the two images in low-frequency fusion. The SAR image does not interfere with the spectral information of the optical image in areas which have opposite polarity in the two images. As described above, the coefficient of the optical image is directly used to be the fused coefficient to maintain spectral information when the average pixel value in 3×3 neighbourhood is close to zero. Therefore, severe spectral distortion doesn't occur in dark areas. In addition, very little SAR noise is introduced in residential areas because of the implementation of the coherence coefficient threshold in high-frequency fusion. A coherence coefficient threshold, 0.8, is set to limit the introduction of noise in residential areas which have high coherence coefficients.

4.2. Objective evaluation

The quantitative evaluation of the results is conducted after subjective visual evaluation. We calculate four quantitative evaluation indicators for all the results obtained with different algorithms including standard deviation, information entropy, mean gradient, and correlation coefficient. The meaning of each indicator is as follows:

- Standard deviation describes the degree of dispersion of pixel values, which measures the degree of contrast of the image. The larger the standard deviation, the higher the contrast ratio.
- Information entropy is the most intuitive standard for reflecting the amount of image information, which represents the amount of information contained in the fused image.
- Mean gradient represents the detail-describing ability of the image.
- Correlation coefficient indicates the degree of correlation between two images. It can be used to measure the spectral-holding degree of the fused image.

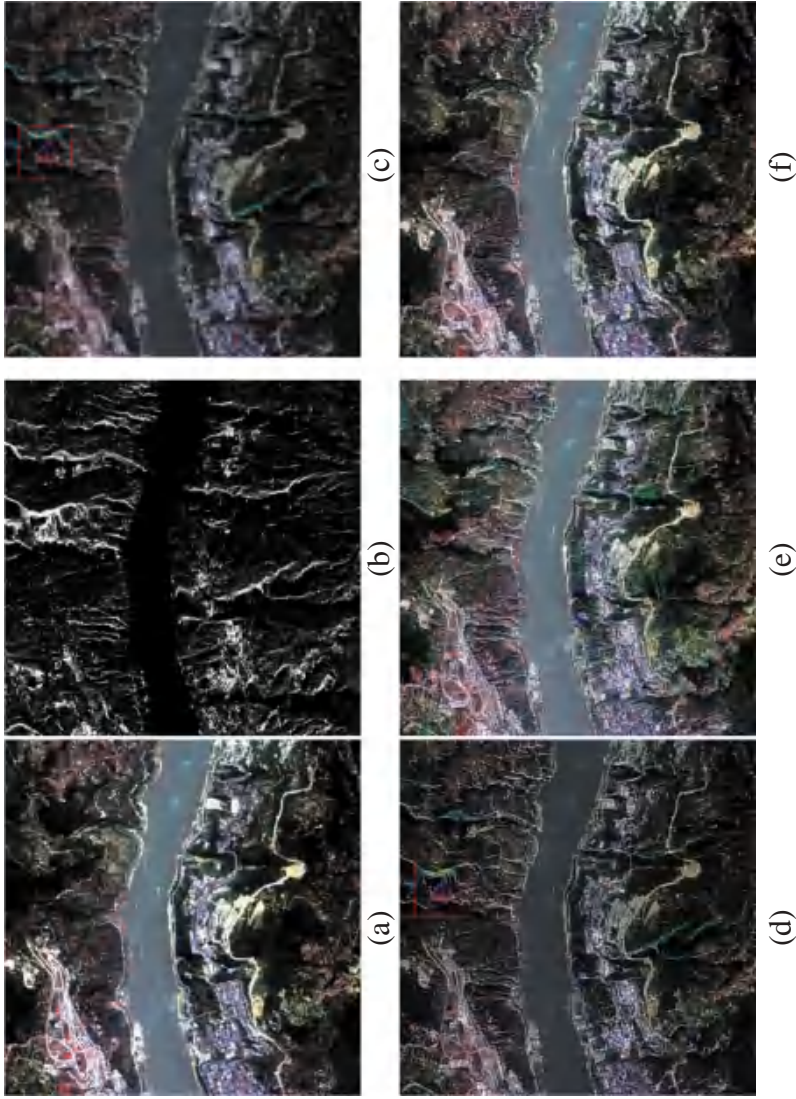


Figure 8. Fusion results of Experiment 2. (a) The original optical image; (b) The original SAR image; (c) Fusion result with NSCT; (d) Fusion result with NSST; (e) Fusion result with the algorithm in Sheng, Yang, and Dong 2018; and (f) Fusion result with our proposed algorithm.

Table 1. Evaluation results of the four algorithms in the two experiments.

Experiment	Method	Standard deviation	Information entropy	Mean gradient	Correlation coefficient
Experiment 1	NSCT	32.9050	6.8013	3.6839	0.8479
	NSST	45.3914	6.8839	9.2850	0.7811
	Sheng	58.5516	7.4782	13.4331	0.8184
	Proposed	59.3896	7.3434	12.3883	0.9006
Experiment 2	NSCT	35.3117	6.9844	2.5905	0.8534
	NSST	47.9846	7.0803	10.4592	0.6957
	Sheng	57.6290	7.5650	14.1942	0.7800
	Proposed	59.7153	7.4780	12.3850	0.9029

Table 1 lists the calculated indicators of the fused images in the two experiments. NSCT has the lowest standard deviation while the proposed algorithm has the highest. It means that NSST is better than NSCT in contrast and visual quality. The proposed algorithm has significant improvement on the basis of NSST and is slightly better than the algorithm in Sheng, Yang, and Dong 2018. For information entropy, NSST is close to NSCT, and the proposed algorithm is better than both of them. It reflects that the fused results with the proposed algorithm contain more information. The algorithm in Sheng, Yang, and Dong 2018 is slightly higher than the proposed algorithm because the results of the algorithm in Sheng, Yang, and Dong 2018 have more noise. As to mean gradient, NSCT is extremely low, and the proposed algorithm is higher than NSCT and NSST, but slightly lower than the algorithm in Sheng, Yang, and Dong 2018. It shows that the proposed algorithm has a better detail-describing ability. In terms of the correlation coefficient, the spectral retention of NSST is slightly weaker than NSCT. But this ability of NSST is improved by our proposed algorithm, which is also better than the algorithm in Sheng, Yang, and Dong 2018.

According to the analysis, compared with NSCT and NSST results, the proposed algorithm in the two experiments has better performance than NSCT and NSST on all the four evaluation indicators. It indicates that the proposed algorithm produces the biggest contrast ratio, the largest amount of information, the most detailed texture, and the most outstanding spectral information preservation in its resultant images. Although the proposed algorithm has a similar effect on the fused images to the algorithm in Sheng, Yang, and Dong 2018, it costs less operating time and introduces less noise.

5. Conclusions

Two major problems in the fusion of SAR and optical images are spectral distortion and excessive introduction of SAR noise. Traditional image fusion technology can't solve the problems. This paper proposes an efficient and novel algorithm based on NSST. To avoid spectral distortion, adaptive weighted averaging based on CV is proposed in low-frequency fusion rule. Thus, the objects which have opposite polarity in the two original images such as rivers maintain their spectral properties well. In addition, this proposed low-frequency fusion rule has a relatively simpler mathematical structure than the algorithm used in Sheng, Yang, and Dong 2018, requiring less operating time and manual work. To deal with the SAR noise problem, a coherence coefficient threshold is set innovatively in high-frequency fusion rule to limit the excessive introduction of SAR noise in residential areas. While this problem was not considered in Sheng, Yang, and

Dong 2018. In the two fusion experiments, the overall quality of the resultant images fused with the proposed algorithms is significantly higher than the other algorithms according to both the visual and the quantitative evaluations. The proposed algorithm proves to be a feasible, useful, innovative, and consistent method for SAR-optical image fusion.

Acknowledgements

And we are very grateful to the European Space Agency for providing Sentinel-2A data for free.

Disclosure statement

No potential conflict of interest was reported by the authors.

Funding

This work was supported by the the Project for Follow-up Work in Three Gorges [2017HXNL-01].

References

- Ban, Y., H. Hu, and I. M. Rangel. 2010. "Fusion of Quickbird MS and RADARSAT SAR Data for Urban Land-Cover Mapping: Object-Based and Knowledge-Based Approach." *International Journal of Remote Sensing* 31 (6): 1391–1410. doi:[10.1080/01431160903475415](https://doi.org/10.1080/01431160903475415).
- Ban, Y., H. Hu, and I. Rangel. 2007. "Fusion of RADARSAT Fine-Beam SAR and QuickBird Data for Land-Cover Mapping and Change Detection." In, edited by W. Ju and S. Zhao, 67522H. doi:[10.1117/12.760747](https://doi.org/10.1117/12.760747).
- Bhatnagar, G., Q. M. J. Wu, and Z. Liu. 2013. "Human Visual System Inspired Multi-Modal Medical Image Fusion Framework." *Expert Systems with Applications* 40 (5): 1708–1720. doi:[10.1016/j.eswa.2012.09.011](https://doi.org/10.1016/j.eswa.2012.09.011).
- Borghys, D., M. Shimoni, and C. Perneel. 2007. "Change Detection in Urban Scenes by Fusion of SAR and Hyperspectral Data." In edited by M. Ehlers and U. Michel, 67490R. doi:[10.1117/12.738767](https://doi.org/10.1117/12.738767).
- Brekke, C., and A. H. S. Solberg. 2005. "Oil Spill Detection by Satellite Remote Sensing." *Remote Sensing of Environment* 95: 1–13. doi:[10.1016/j.rse.2004.11.015](https://doi.org/10.1016/j.rse.2004.11.015).
- Cheng, B., L. Jin, and G. Li. 2018. "Infrared and Visual Image Fusion Using LNSST and an Adaptive Dual-Channel PCNN with Triple-Linking Strength." *Neurocomputing* 310 (October): 135–147. doi:[10.1016/j.neucom.2018.05.028](https://doi.org/10.1016/j.neucom.2018.05.028).
- Da Cunha, A.L., J. Zhou and M. N. Do. 2006. "The Nonsubsampled Contourlet Transform: Theory, Design, and Applications." *IEEE Transactions on Image Processing* 15 (10): 3089–3101. doi:[10.1109/TIP.2006.877507](https://doi.org/10.1109/TIP.2006.877507).
- Do, M. N., and M. Vetterli. 2005. "The Contourlet Transform: An Efficient Directional Multiresolution Image Representation." *IEEE Transactions on Image Processing* 14 (12): 2091–2106. doi:[10.1109/TIP.2005.859376](https://doi.org/10.1109/TIP.2005.859376).
- Easley, G., D. Labate, and W.-Q. Lim. 2008. "Sparse Directional Image Representations Using the Discrete Shearlet Transform." *Applied and Computational Harmonic Analysis* 25 (1): 25–46. doi:[10.1016/j.acha.2007.09.003](https://doi.org/10.1016/j.acha.2007.09.003).
- Errico, A., C. V. Angelino, L. Cicala, G. Persechino, C. Ferrara, M. Lega, A. Vallario, et al. 2015. "Detection of Environmental Hazards through the Feature-Based Fusion of Optical and SAR Data: A Case Study in Southern Italy." *International Journal of Remote Sensing* 36 (13): 3345–3367. doi:[10.1080/01431161.2015.1054960](https://doi.org/10.1080/01431161.2015.1054960).

- Ghahremani, M., and H. Ghassemian. 2015. "Remote-Sensing Image Fusion Based on Curvelets and ICA." *International Journal of Remote Sensing* 36 (16): 4131–4143. doi:10.1080/01431161.2015.1071897.
- Goodman, J. W. 1976. "Some Fundamental Properties of Speckle." *Journal of the Optical Society of America* 66 (11): 1145. The Optical Society. doi:10.1364/josa.66.001145.
- Haghighat, M. B. A., A. Aghagolzadeh, and H. Seyedarabi. 2011. "Multi-Focus Image Fusion for Visual Sensor Networks in DCT Domain." *Computers and Electrical Engineering* 37 (5): 789–797. doi:10.1016/j.compeleceng.2011.04.016.
- Huang, Y., D. Bi, and D. Wu. 2018. "Infrared and Visible Image Fusion Based on Different Constraints in the Non-Subsampled Shearlet Transform Domain." *Sensors* 18 (4): 1169. doi:10.3390/s18041169.
- Joshi, N., M. Baumann, A. Ehammer, R. Fensholt, K. Grogan, P. Hostert, M. Jepsen, et al. 2016. "A Review of the Application of Optical and Radar Remote Sensing Data Fusion to Land Use Mapping and Monitoring." *Remote Sensing* 8 (1): 70. doi:10.3390/rs8010070.
- Kim, S., W.-J. Song, and S.-H. Kim. 2018. "Double Weight-Based SAR and Infrared Sensor Fusion for Automatic Ground Target Recognition with Deep Learning." *Remote Sensing* 10 (2): 72. doi:10.3390/rs10010072.
- Kong, W., L. Zhang, and Y. Lei. 2014. "Novel Fusion Method for Visible Light and Infrared Images Based on NSST-SF-PCNN." *Infrared Physics and Technology* 65: 103–112. Elsevier. doi:10.1016/j.infrared.2014.04.003.
- Li, Q., X. Yang, W. Wei, K. Liu, and G. Jeon. 2018. "Multi-Focus Image Fusion Method for Vision Sensor Systems via Dictionary Learning with Guided Filter." *Sensors* 18 (7): 2143. doi:10.3390/s18072143.
- Li, W., X. Hu, J. Du, and B. Xiao. 2017. "Adaptive Remote-Sensing Image Fusion Based on Dynamic Gradient Sparse and Average Gradient Difference." *International Journal of Remote Sensing* 38 (23): 7316–7332. doi:10.1080/01431161.2017.1371863.
- Sheng, J., X. Yang, and Z. Dong. 2018. "Fusion of SAR and Visible Images Based on NSST-IHS and Sparse Representation." *Journal of Graphics* 39 (2): 201–208. doi:10.11996/JGJ.2095-302X.2018020201.
- Singh, S., R. S. A. Deep Gupta, and V. Kumar. 2015. "Nonsubsampled Shearlet Based CT and MR Medical Image Fusion Using Biologically Inspired Spiking Neural Network." *Biomedical Signal Processing and Control* 18: 91–101. Elsevier Ltd. doi:10.1016/j.bspc.2014.11.009.
- Stępnia, C. 2011. "Coefficient of Variation." In *International Encyclopedia of Statistical Science*, 267. Berlin Heidelberg: Springer. doi:10.1007/978-3-642-04898-2_177.
- Tang, Z., J. Wang, and S. Huang. 2000. "Wavelet Transform Application for Image Fusion." In edited by H. H. Szu, M. Vetterli, W. J. Campbell, and J. R. Buss, 462–469. doi:10.1117/12.381706.
- Wang, H., and C. Glennie. 2015. "Fusion of Waveform LiDAR Data and Hyperspectral Imagery for Land Cover Classification." *ISPRS Journal of Photogrammetry and Remote Sensing* 108 (October): 1–11. Elsevier B.V. . doi:10.1016/j.isprsjprs.2015.05.012.
- Wang, J., J. Peng, X. Jiang, X. Feng, and J. Zhou. 2017. "Remote-Sensing Image Fusion Using Sparse Representation with Sub-Dictionaries." *International Journal of Remote Sensing* 38 (12): 3564–3585. doi:10.1080/01431161.2017.1302106.
- Yi, W., Y. Zeng, and Z. Yuan. 2018. "Fusion of GF-3 SAR and Optical Images Based on the Nonsubsampled Contourlet Transform." *Acta Optica Sinica* 38 (11): 1110002. Chinese Optical Society. doi:10.3788/AOS201838.1110002.
- Zhang, L., and J. Zhang. 2018. "A Novel Remote-Sensing Image Fusion Method Based on Hybrid Visual Saliency Analysis." *International Journal of Remote Sensing* 39 (22): 7942–7964. doi:10.1080/01431161.2018.1479791.
- Zhang, X., J. Ren, Z. Huang, and F. Zhu. 2016. "Spiking Cortical Model Based Multimodal Medical Image Fusion by Combining Entropy Information with Weber Local Descriptor." *Sensors* 16 (9): 1503. doi:10.3390/s16091503.